A&A, 712, L13 (2026)
https://doi.org/10.1051/0004-6361/202661622

Astronomy & Astrophysics

Letter to the Editor

A quiet host in an active planet-forming disk: Optical spectroscopy of WISPIT 2

C. Swastik[1,⋆], M. Bestha[2,⋆⋆], L. S. Sonith[2,⋆⋆], S. Facchini[1], T. Sivarani[2], R. K. Banyal[2], Z. Wahhaj[3], A. Choudhary[5], M. Gopinathan[2], P. Saraf[4], A. Mallick[6], M. P. Navaneeth[2], S. Biswas[2], and K. Khushbu[2]

[1] Dipartimento di Fisica, Università degli Studi di Milano, Via Celoria 16, 20133 Milano, Italy
[2] Indian Institute of Astrophysics, II Block, Koramangala, Bengaluru 560034, India
[3] European Southern Observatory, Alonso de Córdova 3107, Vitacura Casilla 19001, Santiago, Chile
[4] Physical Research Laboratory, Navrangpura, Ahmedabad 380009, India
[5] Indian Institute of Technology (Indian School of Mines) Dhanbad, Dhanbad 826004, Jharkhand, India
[6] Tata Institute of Fundamental Research, Homi Bhabha Road, Colaba, Mumbai 400005, India

Received 23 June 2026 / Accepted 15 July 2026

ABSTRACT

Context. WISPIT 2 is a young pre-main-sequence star hosting a multi-ringed transition disk and two directly imaged protoplanets. One of them, WISPIT 2b, has been confirmed to be accreting. This makes WISPIT 2 the closest known analogue to PDS 70; however, prior to this work, no optical spectrum of the central star had been published. Population-synthesis models predict that stellar accretion can be strongly suppressed once two or more giant planets have formed, so characterising the atmospheric and accretion properties of such hosts is essential.

Aims. We present the first optical spectrum of WISPIT 2 and use it to derive the host atmospheric parameters, test its youth spectroscopically, and constrain its stellar accretion state relative to PDS 70 and to the embedded planets.

Methods. We analysed low-resolution HFOSC spectra ($R \sim 1200$ for Grism 7 and $R \sim 2200$ for Grism 8) from the 2-m Himalayan Chandra Telescope with `iSpec`, validating the pipeline at HFOSC resolution against Gaia FGK Benchmark Stars and K-type pre-main-sequence templates from the public Manara et al. library. The Hα residual filling was measured relative to synthetic photospheric profiles and compared with the expected chromospheric-noise level.

Results. Hα remains in net absorption, but is partially filled in by emission; the weak residual filling (1.5–2.0σ) lies ~1 dex below the chromospheric-noise level, consistent with chromospheric emission and no detectable accretion. We place a 95% upper limit $\dot{M}_{\rm acc} < 3.6 \times 10^{-11}\,M_\odot\,{\rm yr}^{-1}$, below even the lowest epoch of PDS 70's monitoring and implying a host-to-planet ratio $\dot{M}_\star/\dot{M}_{2b} \lesssim 18$. We also measure $T_{\rm eff} = 4551 \pm 150$ K and a first, low-resolution, model-dependent global metallicity [M/H] = -0.17 ± 0.16; the surface gravity and Li I equivalent width (EW) support the pre-main-sequence nature of the host.

Conclusions. Both known double-protoplanet hosts, PDS 70 and WISPIT 2, therefore appear to show strongly suppressed or undetectable stellar accretion. Larger spectroscopic samples are needed to test whether this is common in multi-protoplanet transition disks.

Key words. planets and satellites: gaseous planets – stars: abundances

1. Introduction

Direct imaging of an accretingprotoplanet embedded in its natal disk is exceptionally rare; it requires a young gas-rich transition disk, a planet accreting strongly enough to outshine the disk in Hα, and a favourable geometry. Only a handful of candidates have been confirmed by direct Hα detection (Haffert et al. 2019; Close et al. 2025), and only two systems host more than one directly imaged protoplanet: PDS 70 (Keppler et al. 2018; Haffert et al. 2019) and (since 2025) WISPIT 2 (van Capelleveen et al. 2025; Close et al. 2025; Lawlor & van Capelleveen 2026), making WISPIT 2 the closest known analogue to PDS 70. VLT/SPHERE imaging revealed an extended multi-ringed disk around a ~5 Myr, ~1.08 $M_\odot$ pre-main-sequence (PMS) star with an accreting ~5 $M_{\rm Jup}$ protoplanet (WISPIT 2b) at ~57 au (van Capelleveen et al. 2025); MagAO-X confirmed its Hα accretion (Close et al. 2025); VLTI/GRAVITY revealed a second embedded companion (WISPIT 2c, ~8–12 $M_{\rm Jup}$ at ~15 au) (Lawlor & van Capelleveen 2026); and ALMA Band 7 resolved a narrow millimetre dust ring at 144 au, interior to which WISPIT 2b orbits (Facchini et al. 2026). The discovery of two giant protoplanets in one disk makes it possible to test how accretion is divided between the star and the planets. In single-protoplanet systems, gas is expected to leak past the gap-opening planet and accrete onto the star near the canonical T Tauri value, but whether this persists with multiple giant planets is unclear. PDS 70 provides one data point, its host accreting more than an order of magnitude below the canonical rate (Thanathibodee et al. 2020; Manara et al. 2023); whether this suppression is generic to multi-protoplanet hosts or specific to PDS 70 cannot be settled without a comparable measurement on a second system. The central star of WISPIT 2 remains poorly characterised, with the parameters of van Capelleveen et al. (2025) deriving from Gaia astrometry

⋆ Corresponding author: swastik.chowbay@unimi.it
⋆⋆ M. Bestha and L. S. Sonith contributed equally to this work.

and photometry and no published optical spectrum. In this Letter we present the first optical spectrum of WISPIT 2, obtained with HFOSC[1] on the 2-m Himalayan Chandra Telescope, and use it to derive the host atmospheric parameters and a low-resolution global [M/H] in the same `iSpec` framework applied to PDS 70 (Swastik et al. 2021, PDS 70: [Fe/H] $= -0.11 \pm 0.01$), to test the system's youth for lithium, and to constrain the host accretion state from Hα. Given the modest resolution and PMS nature, we validate the methodology against Gaia FGK Benchmark Stars and K-type PMS empirical templates (Manara et al. 2017), both degraded to HFOSC resolution. We detect no stellar accretion and place an upper limit a factor of a few below PDS 70's central rate and well below the canonical T Tauri rate, so both known double-protoplanet hosts appear to show strongly suppressed or undetectable host accretion.

2. Observations and data reduction

WISPIT 2[2] (RA = $19^{\rm h}\,23^{\rm m}\,17.03^{\rm s}$, Dec = $-07°\,40'\,55.1''$, J2000; $V = 11.60 \pm 0.12$ mag) was observed on UT 2026-04-14 with the HFOSC spectrograph on the 2-m Himalayan Chandra Telescope at Hanle, under a Director's Discretionary Time allocation, using the $1.92''$-wide long slit (wider than the typical Hanle seeing, to minimise wavelength-dependent slit losses). One 600 s Grism 7 exposure (~3800–7700 Å, $R \sim 1200$) was followed by three Grism 8 exposures (~5200–9300 Å, $R \sim 2200$; 600, 600, 300 s), with Feige 34 observed the same night for flux calibration.

The data were reduced with standard `IRAF` routines (bias subtraction, flat-fielding, `lacos_spec` cosmic-ray rejection, optimal extraction), wavelength-calibrated against FeAr/FeNe arcs (rms ~0.1 pixel) and response-corrected using Feige 34. The resulting Grism 7 and Grism 8 spectra were combined and scaled to match the ASAS-SN g-band magnitude obtained from the light curve (Shappee et al. 2014; Kochanek et al. 2017), thereby placing them on an absolute flux scale. The three Grism 8 frames are the primary dataset for all the measurements: they resolve the narrow Hα and Li I 6708 Å diagnostics, cover the Ca II infrared triplet, and provide a frame-to-frame scatter estimate. The Grism 7 frame serves only as a broadband-continuum check (Fig. A.1). Each spectrum was placed on the stellar rest frame by cross-correlating against a Castelli/ATLAS9 K-dwarf template ($T_{\rm eff} \simeq 4550$ K, $\log g \simeq 4.3$, [M/H]= 0) broadened to HFOSC resolution, removing the residual ~0.1–0.2 pixel arc zero-point; this is important for the absolute Hα EW (Sect. 3.3), but is negligible for the broadband fits. Spectra were continuum-normalised by a cubic-spline fit over ~50 line-free windows and median-combined within each grism. The combined Grism 8 spectrum reaches a continuum S/N per resolution element of ~350–370 across 5700–8000 Å; the telluric bands were masked.

[1] Himalayan Faint Object Spectrograph Camera; https://www.iiap.res.in/centers/iao/facilities/hct/

[2] WISPIT 2 is the likely optical counterpart of the RASS X-ray source RX J1923.2–0740 (Moran 1996, their Table 2), providing an independent indicator of youth, consistent with the Li-rich, K-type RASS-selected young stars found around nearby star-forming regions (Alcalá et al. 1995; Krautter et al. 1997).

3. Results

3.1. Optical spectrum

The combined continuum-normalised HFOSC spectrum (Fig. A.1, Appendix A) is that of a late-type K dwarf: the G-band, the Mg I b triplet, the Na I D doublet, Li I 6708 Å, and the Ca II infrared triplet are all detected in absorption. The Ca II IRT cores appear somewhat shallower than is typical for a quiescent K3–K4V dwarf, tentatively suggesting weak chromospheric core infilling; we do not use the IRT cores as an accretion diagnostic at this resolution.

3.2. Atmospheric parameters

We derived the atmospheric parameters with `iSpec` (Blanco-Cuaresma et al. 2014), following Swastik et al. (2021), using only the median-combined Grism 8 spectrum. This grism provides the higher-resolution red-optical range used for the fit. The Grism 7 spectrum was excluded from the atmospheric-parameter inference and was used only as a broadband-continuum check. We performed spectral synthesis with SPECTRUM (Gray & Corbally 1994) on the Castelli/ATLAS9 grid (Castelli & Kurucz 2003), sampling the joint posterior on $T_{\rm eff}$, $\log g$, and [M/H] by a Markov chain Monte Carlo (MCMC) algorithm over 6200–8000 Å with chromospheric, accretion-sensitive, and telluric regions masked. Informative priors on $T_{\rm eff}$ ($\sigma = 400$ K) and $\log g$ ($\sigma = 0.3$ dex) from van Capelleveen et al. (2025) break the $T_{\rm eff}$–$\log g$ degeneracy; [M/H] carries no prior. Veiling is expected to be negligible for any plausible accretion rate consistent with the Hα non-detection (Sect. 3.3), so we adopted a veiling-free model; an a posteriori check using the upper limit from Sect. 3.4 gives $r_{6000} \lesssim 0.01$, confirming the assumption. The fit is unimodal with reduced $\chi^2_\nu = 0.72$ (Appendix A). Because $R \sim 2200$ is below the resolution regime where `iSpec` is usually applied, and because WISPIT 2 is a PMS star, we validated the pipeline against five Gaia FGK benchmark stars and five K-type PMS empirical templates, both degraded to the HFOSC dispersion and resolution. All validation spectra were processed with the identical `iSpec` configuration used for WISPIT 2. The recovered parameters and systematic-error budget are detailed in Appendix B. These tests support a robust temperature scale at the ~150–180 K level, while showing that $\log g$ and [M/H] are less precise at HFOSC resolution. The PMS templates test the behaviour of young K-star spectra, but do not provide independent metallicity standards, so we define the [M/H] systematic from the GBS comparison and treat [M/H] as a low-resolution, model-dependent global estimate. For WISPIT 2 the analysis yields $T_{\rm eff} = 4551 \pm 150$ K, $\log g = 4.32 \pm 0.18$, and [M/H] $= -0.17 \pm 0.16$ (uncertainties dominated by the validation floor). The temperature agrees within the floor with the photometric 4400 ± 50 K of van Capelleveen et al. (2025), confirming the K3–K4 classification. Combining $T_{\rm eff}$ with the SED luminosity $L_\star = 0.699 \pm 0.021\,L_\odot$ (van Capelleveen et al. 2025) gives $R_\star = 1.34 \pm 0.09\,R_\odot$, which with the stellar mass $M_\star = 1.08\,M_\odot$ (van Capelleveen et al. 2025) implies $\log g \simeq 4.22$, in agreement with the spectroscopic value within the systematic floor; we do not bias-correct $\log g$ for the benchmark calibration offset (Appendix B) and adopt $R_\star = 1.34\,R_\odot$ throughout. The metallicity, the only parameter without an informative prior, is the first low-resolution spectroscopic estimate for the system; we treat it as a model-dependent global metallicity rather than a precise abundance. Two further consistency checks on these parameters (an independent $T_{\rm eff}$ estimate from the Na I D equivalent width and an extinction check from the flux-calibrated slope) are described in Appendix C.

3.3. Hα and the stellar accretion state

Hα at 6562.8 Å remains in net absorption, with no resolved emission core (Fig. 1). From the three flux-calibrated Grism 8 exposures, combined into an inverse-variance-weighted mean on a common rest-frame grid, we measured the equivalent width by direct integration over 6555–6570 Å against a local linear pseudo-continuum (6520–6545 and 6580–6605 Å side-bands), adopting the convention that positive EW denotes net absorption. Per-pixel noise, continuum-window variation (±5 Å), and per-frame scatter were propagated by MCMC methods. The rest-frame alignment was verified against two clean Fe I lines flanking Hα. This yields $\mathrm{EW}_{\mathrm{H}\alpha,\mathrm{obs}} = +0.395 \pm 0.011$ Å, with a continuum flux density $F_{\mathrm{cont}}(6562.8\,\text{Å}) = (1.375 \pm 0.038) \times 10^{-13}$ erg s^{-1} cm^{-2} Å^{-1} (the ∼3% internal scatter). The absolute flux scale is anchored to the ASAS-SN g-band photometry (Appendix C), leaving a residual absolute-calibration uncertainty of ∼5% (the scaling uncertainty), i.e. ∼0.02 dex in $\log L_{\mathrm{acc}}$, sub-dominant to the photospheric EW systematic. To estimate the photospheric Hα contribution, we synthesised the line region with iSpec at the posterior-median parameters (Sect. 3.2), using two independent grids (Castelli/ATLAS9 (Castelli & Kurucz 2003) and MARCS GES (Gustafsson et al. 2008; Heiter et al. 2021)) to make the model-atmosphere dependence explicit. For each grid, $N = 1000$ Monte Carlo syntheses were drawn from the benchmark systematic floors ($\sigma(T_{\mathrm{eff}}) = 150$ K, $\sigma(\log g) = 0.18$, $\sigma([\mathrm{M/H}]) = 0.16$ dex; Sect. 3.2), with identical draws for both grids. The EW is dominated by the T_{eff} systematic; $\log g$ and [M/H] contribute negligibly. The two grids give $\mathrm{EW}_{\mathrm{phot}}^{\mathrm{Castelli}} = 0.608 \pm 0.146$ Å and $\mathrm{EW}_{\mathrm{phot}}^{\mathrm{MARCS}} = 0.682 \pm 0.144$ Å (16th–84th percentile spread), kept separate so the model-atmosphere dependence is explicit. The excess $\mathrm{EW}_{\mathrm{exc}} = \mathrm{EW}_{\mathrm{phot}} - \mathrm{EW}_{\mathrm{obs}}$ is then +0.213 ± 0.147 Å (Castelli) and +0.287 ± 0.144 Å (MARCS): positive for both grids, but grid-dependent in significance, 1.45σ and 1.98σ respectively, the observed EW being ∼35–42% weaker than predicted. We therefore regard the Hα residual filling as weak and model-dependent: consistent in sign across both atmosphere grids, but not cleanly separable from chromospheric activity. As we show in Sect. 3.4, this filling lies ∼1.1 dex below the Manara et al. (2013) chromospheric noise expected at this T_{eff}, so its accretion-luminosity equivalent is consistent with chromospheric emission alone and yields only an upper limit on the stellar accretion rate.

The inferred ∼0.2–0.3 Å of equivalent filling is far below the |EW| > 3 Å classical T Tauri threshold (White & Basri 2003), nominally a weak-line T Tauri star, though the structured disk and directly imaged protoplanets, including the accreting WISPIT 2b, confirm that substantial circumstellar material remains.

3.4. Stellar accretion rate

For reference, and to set an upper limit, we converted the Hα residual filling into an accretion luminosity with the Alcalá et al. (2017) calibration, propagating all uncertainties (photospheric-EW systematic, observed EW and continuum flux, extinction, distance, and calibration scatter) through a Monte Carlo algorithm; the full derivation is given in Appendix D. The dereddened excess gives $\log L_{\mathrm{acc}}/L_{\odot} = -3.54^{+0.26}_{-0.37}$, which lies ≃ 1.1 dex below the Manara et al. (2013) chromospheric-noise level expected at this T_{eff}. The residual Hα filling is therefore fully consistent with chromospheric emission, and combined with its low significance (1.5–2.0σ) we treat the Hα-derived L_{acc} purely as an upper limit, $\dot{M}_{\mathrm{acc}} < 3.6 \times 10^{-11}\,M_{\odot}\,\mathrm{yr}^{-1}$ (95%), far below the canonical 10^{-8}–$10^{-9}\,M_{\odot}\,\mathrm{yr}^{-1}$ CTTS rate (Manara et al. 2023): host accretion is undetectable in this spectrum. The single-epoch measurement may also differ from the time-averaged rate given typical CTTS variability.

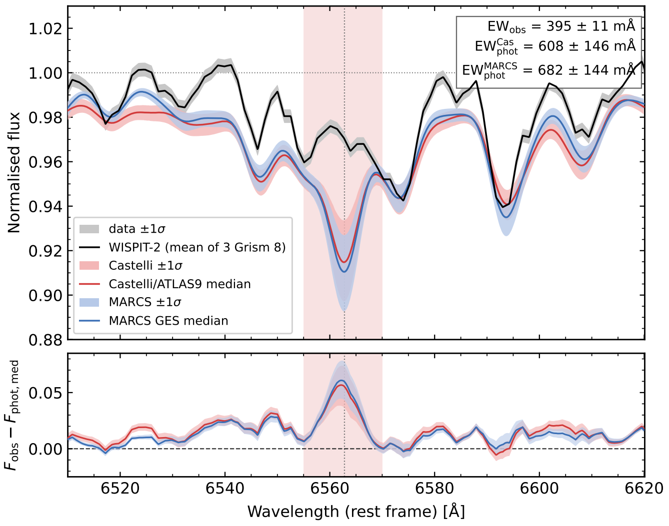

Fig. 1. Top: Normalised Hα region of WISPIT 2 (black; mean of three Grism 8 exposures, ±1σ in grey), with iSpec photospheric syntheses from the Castelli/ATLAS9 (red) and MARCS GES (blue) grids at the posterior-median parameters. The coloured bands give the ±1σ Monte Carlo envelope. The shaded vertical band marks the 6555–6570 Å EW integration window. Bottom: Residuals $F_{\mathrm{obs}} - F_{\mathrm{phot}}$ for each grid, showing the residual Hα filling relative to the photospheric models. The two grids trace each other closely, but are systematically offset, giving excess significances of 1.45σ (Castelli) and 1.98σ (MARCS).

3.5. Lithium and stellar youth

The Li I 6708 Å doublet is clearly detected. We measured EW(Li + Fe) = 0.344 ± 0.030 Å and inferred EW(Li) = 0.334 ± 0.030 Å after applying a 10 mÅ blend correction, supporting the independently inferred youth of the star. At HFOSC resolution the corrected EW should still be regarded as an approximate upper limit because of unresolved Fe I/CN features, so it does not constrain the precise age (Appendix E).

4. Discussion

PDS 70, whose two directly imaged protoplanets are both confirmed to be accreting and whose host was characterised with the same `iSpec` framework (Swastik et al. 2021), is the natural benchmark. WISPIT 2 is hotter (4551 vs. 4152 K) and the two hosts have comparable mildly sub-solar metallicities (−0.17 vs. −0.11 dex); with $N = 2$ we infer no metallicity preference. WISPIT 2 and PDS 70 compare closely in accretion as well. PDS 70's host accretes at $\sim 10^{-10}\,M_{\odot}\,\mathrm{yr}^{-1}$ ($\log \dot{M}_{\mathrm{acc}} \approx -10.06$; Campbell-White et al. 2023), with monitoring spanning 0.6–$2.2 \times 10^{-10}\,M_{\odot}\,\mathrm{yr}^{-1}$ (Thanathibodee et al. 2020), already over an order of magnitude below the canonical 10^{-8}–$10^{-9}\,M_{\odot}\,\mathrm{yr}^{-1}$ rate for solar-mass T Tauri stars (Manara et al. 2023). As both hosts have transition disks, the more appropriate comparison is with transition-disk hosts of similar mass; these overlap the CTTS distribution, but tend somewhat lower, though not significantly (Manara et al. 2023); even so, the WISPIT 2 limit sits at the extreme low-accretion end. Our upper limit is a factor of ~3 below PDS 70's central rate and below even the lowest epoch of its monitoring (Thanathibodee et al. 2020); with the Hα filling ~1.1 dex below the chromospheric noise floor (Manara et al. 2013), it is consistent with pure chromospheric emission and we detect no accretion. Both systems (two embedded gas giants in a structured transition disk around a young roughly solar-mass star) thus appear to show strongly suppressed or undetectable host accretion, on the suppressed-accretion side of a mixed theoretical picture in which gap-opening giants are expected to let gas leak onto the star (Lubow & D'Angelo 2006; Dürmann & Kley 2015); however, population-synthesis models predict substantial suppression once two or more giants have formed (Manara et al. 2019). The suppression may indicate that multi-protoplanet disks enter a distinct gas-transport regime of serial filtering, with the outer companion intercepting part of the inflow and the inner companion perturbing the residual, so that overlapping gaps attenuate the channels feeding the star. However, two-planet hydrodynamical simulations give a more conservative picture, in which gas can still diffuse through the gaps efficiently and a second accreting planet need not suppress stellar accretion by more than a factor of a few (Bergez-Casalou et al. 2023). Whether serial filtering alone explains the suppression thus remains an open question; additional unresolved planets, inefficient gap-crossing flow, or inner-disk dispersal may be required, and resolved inner-disk gas observations (e.g. with ALMA) would provide a direct test.

The host rate can also be compared with the planetary rates. Close et al. (2025) measured $\dot{M}_{2b} \sim 2 \times 10^{-12}\, M_\odot\,\mathrm{yr}^{-1}$ for WISPIT 2b, so even our upper limit implies $\dot{M}_\star/\dot{M}_{2b} \lesssim 18$, and the true ratio may be far smaller. This contrasts sharply with ordinary CTTS, where stellar rates exceed protoplanetary ones by three to four orders of magnitude; the rates are non-contemporaneous and differently calibrated, so the ratio is uncertain at the factor-of-several level, but the much smaller contrast is robust and consistent with the protoplanets intercepting much of the inflow.

5. Conclusions

From the first optical spectrum of WISPIT 2 we derived T_eff = 4551 ± 150 K, $\log g = 4.32 \pm 0.18$, and a low-resolution, model-dependent [M/H] = -0.17 ± 0.16 dex, validated at HFOSC resolution against Gaia FGK benchmark stars and K-type PMS templates (Manara et al. 2017); the gravity and lithium EW are consistent with a pre-main-sequence K star. Hα shows only weak (1.5–2.0σ) residual filling, ~1.1 dex below the chromospheric noise floor (Manara et al. 2013), and hence consistent with pure chromospheric emission, so we detected no accretion and set a 95% upper limit $\dot{M}_\mathrm{acc} < 3.6 \times 10^{-11}\, M_\odot\,\mathrm{yr}^{-1}$, a factor of a few below PDS 70's central rate and below even the lowest epoch of its monitoring (Thanathibodee et al. 2020). WISPIT 2 thus joins PDS 70 as a double-protoplanet host with strongly suppressed or undetectable accretion; with $N = 2$ this is suggestive rather than established. A multi-epoch $R \gtrsim 10\,000$ spectrum would resolve Hα and separate accretion from chromospheric emission, and an ALMA measurement of the inner gas reservoir would test whether gas is retained, filtered, or depleted in the inner disk.

6. Data availability

The reduced HFOSC spectra of WISPIT 2 in FITS format are available at the CDS via `https://cdsarc.cds.unistra.fr/viz-bin/cat/J/A+A/712/L13`.

Acknowledgements. We thank the staff of the Indian Astronomical Observatory, Hanle, and CREST, Hosakote, operated by the Indian Institute of Astrophysics, for support during the HCT observations, and the ICTS program EXOPLANETS2026 (ICTS/EXOPLANETS2026/03). S.C. is funded by the European Union (ERC, UNVEIL, 101076613); views and opinions expressed are those of the authors only and do not necessarily reflect those of the European Union or the European Research Council, and neither can be held responsible for them. S.C. acknowledges PRIN-MUR 2022YP5ACE. We thank Carlo Manara for insightful comments and Ajay Saini and Srikant Bhandari for taking the observations and sending us the data promptly. This work used `IRAF`, `iSpec` (Blanco-Cuaresma et al. 2014), `SPECTRUM` (Gray & Corbally 1994), `astropy`, `numpy`, `scipy`, and `emcee`. C.S. fondly remembers Lalu, a dear companion who now is in the land of unknown and whose presence brightened the months this work was carried out.

References

Alcalá, J. M., Krautter, J., Schmitt, J. H. M. M., et al. 1995, A&AS, 114, 109
Alcalá, J. M., Manara, C. F., Natta, A., et al. 2017, A&A, 600, A20
Bergez-Casalou, C., Bitsch, B., Kurtovic, N. T., & Pinilla, P. 2023, A&A, 669, A129
Blanco-Cuaresma, S., Soubiran, C., Heiter, U., & Jofré, P. 2014, A&A, 569, A111
Bouvier, J., Barrado, D., Moraux, E., et al. 2018, A&A, 613, A63
Campbell-White, J., Manara, C. F., Benisty, M., et al. 2023, ApJ, 956, 25
Castelli, F., & Kurucz 2003, in Modelling of Stellar Atmospheres, eds. N. Piskunov, W. W. Weiss, & D. F. Gray, IAU Symp., 210, A20
Close, L. M., van Capelleveen, R. F., Weible, G., et al. 2025, ApJ, 990, L9
Dürmann, C., & Kley, W. 2015, A&A, 574, A52
Facchini, S., Curone, P., Benisty, M., et al. 2026, ApJ, 998, L16
Gray, R. O., & Corbally, C. J. 1994, AJ, 107, 742
Gustafsson, B., Edvardsson, B., Eriksson, K., et al. 2008, A&A, 486, 951
Haffert, S. Y., Bohn, A. J., de Boer, J., et al. 2019, Nat. Astron., 3, 749
Heiter, U., Lind, K., Bergemann, M., et al. 2021, A&A, 645, A106
Jofré, P., Heiter, U., Soubiran, C., et al. 2014, A&A, 564, A133
Keppler, M., Benisty, M., Müller, A., et al. 2018, A&A, 617, A44
Kochanek, C. S., Shappee, B. J., Stanek, K. Z., et al. 2017, PASP, 129, 104502
Krautter, J., Wichmann, R., Schmitt, J. H. M. M., et al. 1997, A&AS, 123, 329
Lawlor, C., & van Capelleveen, R. F. 2026, ApJ, [2603.22085]
Lubow, S. H., & D'Angelo, G. 2006, ApJ, 641, 526
Manara, C. F., Testi, L., Rigliaco, E., et al. 2013, A&A, 551, A107
Manara, C. F., Frasca, A., Alcalá, J. M., et al. 2017, A&A, 605, A86
Manara, C. F., Mordasini, C., Testi, L., et al. 2019, A&A, 631, L2
Manara, C. F., Ansdell, M., Rosotti, G. P., et al. 2023, in Protostars and Planets VII, eds. S. Inutsuka, Y. Aikawa, T. Muto, K. Tomida, & M. Tamura, ASP Conf. Ser., 534, 539
Martín, E. L., et al. 1997, A&A, 318, 805
Moran, E. C., et al. 1996, ApJS, 106, 341
Shappee, B. J., Prieto, J. L., Grupe, D., et al. 2014, ApJ, 788, 48
Somers, G., & Pinsonneault, M. H. 2017, ApJ, 850, 134
Soubiran, C., Creevey, O. L., Lagarde, N., et al. 2024, A&A, 682, A145
Swastik, C., Banyal, R. K., Narang, M., et al. 2021, AJ, 161, 114
Thanathibodee, T., Calvet, N., Bae, J., Muzerolle, J., & Hernández, R. F. 2020, ApJ, 892, 81
Tripicchio, A., Severino, G., Covino, E., Terranegra, L., & Garcia Lopez, R. J. 1997, A&A, 327, 681
van Capelleveen, R. F., Ginski, C., Kenworthy, M. A., et al. 2025, ApJ, 990, L8
White, R. J., & Basri, G. 2003, ApJ, 582, 1109

Appendix A: Combined optical spectrum and atmospheric-parameter fit

The continuum-normalised HFOSC spectrum and the atmospheric-parameter fit are summarised in Figs. A.1–A.3. The posterior is unimodal, with the expected positive correlations of $T_{\rm eff}$ with $\log g$ and [M/H]. Its formal widths do not include the validation-based systematic floors adopted in Sect. 3.2.

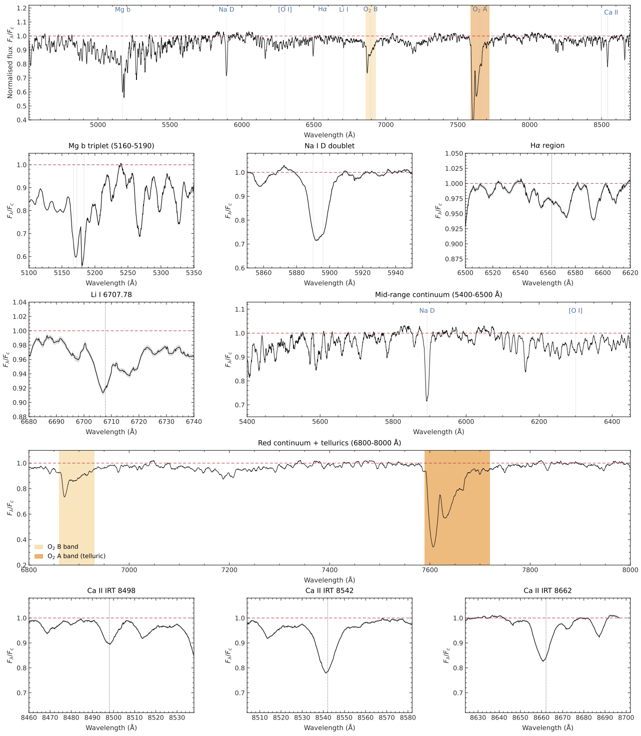

Fig. A.1. Combined continuum-normalised HFOSC spectrum of WISPIT 2 (Grism 7 + Grism 8, 2026 April 14). Grism 7 is used below 5180 Åand Grism 8 above it. The panels identify the principal photospheric diagnostics, Hα, Li I 6708 Å, the Ca II infrared triplet, and the O_2 telluric bands.

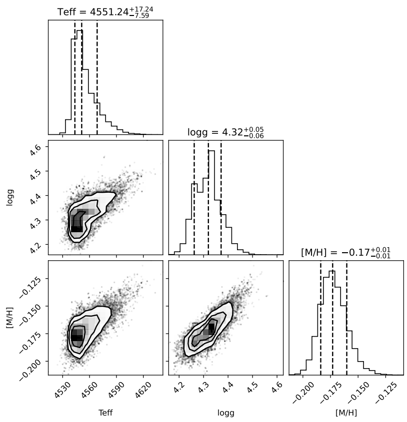

Fig. A.2. MCMC posterior for $T_{\rm eff}$, $\log g$, and [M/H]. The dashed lines mark the 16th, 50th, and 84th percentiles.

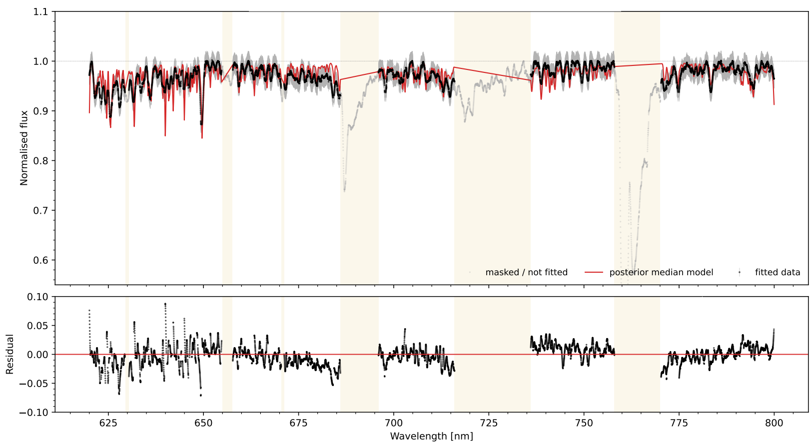

Fig. A.3. Median-combined Grism 8 spectrum (black) and best-fit `iSpec` model (red) for $T_{\rm eff}$ = 4551 K, $\log g$ = 4.32, and [M/H] = −0.17. The grey regions were excluded from the fit. The fit has χ^2_ν = 0.72 and a residual RMS of 1.66%.

Appendix B: Benchmark validation of the iSpec pipeline

We validated the analysis using five Gaia FGK benchmark stars (GBS) and five K-type PMS templates from the public Manara et al. libraries (Manara et al. 2017), degraded and analysed with the same settings used for WISPIT 2.

Table B.1. GBS validation of the iSpec pipeline at HFOSC resolution.

Star	$T_{\rm ref}$	$T_{\rm fit}$	ΔT	$g_{\rm ref}$	$g_{\rm fit}$	Δg	[Fe/H]$_{\rm ref}$	[Fe/H]$_{\rm fit}$	Δ[Fe/H]
HIP 12114	4583	4686 ± 25	+103	4.52	4.73 ± 0.04	+0.21	−0.17	−0.19 ± 0.07	−0.02
HIP 104214	4398	4533 ± 21	+135	4.63	4.77 ± 0.04	+0.14	−0.33	−0.24 ± 0.06	+0.09
HIP 114622	4800	4677 ± 26	−123	4.55	4.77 ± 0.04	+0.22	+0.04	−0.07 ± 0.07	−0.11
HIP 108870	4676	4667 ± 30	−9	4.59	4.77 ± 0.04	+0.18	−0.08	−0.15 ± 0.08	−0.07
HIP 73184	4657	4586 ± 28	−71	4.60	4.77 ± 0.04	+0.17	+0.03	−0.03 ± 0.07	−0.06

Table B.2. PMS-template validation using K-type empirical spectra degraded to HFOSC resolution.

Object	$T_{\rm ref}$ (K)	$T_{\rm fit}$ (K)	ΔT (K)	$g_{\rm ref}$	$g_{\rm fit}$	Δg	[M/H]$_{\rm fit}$
RXJ1538.6−3916	4522 ± 127	4654 ± 16	+132	4.21 ± 0.13	4.11 ± 0.03	−0.10	+0.22 ± 0.01
RXJ1543.1−3920	4308 ± 107	4429 ± 15	+121	4.12 ± 0.23	4.23 ± 0.05	+0.11	+0.17 ± 0.01
RXJ1547.7−4018	4971 ± 75	4793 ± 19	−178	4.22 ± 0.16	4.07 ± 0.05	−0.15	+0.10 ± 0.01
RXJ0438.6+1546	4915 ± 170	4792 ± 15	−123	4.12 ± 0.30	4.42 ± 0.04	+0.30	+0.14 ± 0.01
RXJ1515.8−3331	4997 ± 71	4920 ± 11	−77	3.86 ± 0.25	4.29 ± 0.01	+0.43	+0.04 ± 0.01

Notes. GBS reference $T_{\rm eff}$ and $\log g$ values are from Soubiran et al. (2024), and [Fe/H] from Jofré et al. (2014); recovered uncertainties are formal posterior widths. The offsets motivate floors of 150 K in $T_{\rm eff}$ and 0.16 dex in [M/H], while the coherent +0.18 ± 0.03 dex gravity offset is used as a floor rather than a correction. The PMS median absolute offsets are 123 K and 0.15 dex in $T_{\rm eff}$ and $\log g$. Their [M/H] values are only a near-solar consistency check because the templates are not metallicity standards. Veiling was fixed to zero, consistent with $r_{6000} \lesssim 0.01$.

Appendix C: Flux-calibration, temperature, and extinction checks

The response-corrected spectra were scaled to the ASAS-SN g-band light curve (Shappee et al. 2014; Kochanek et al. 2017); the required factor was 2.856 ± 0.137. The EWs are invariant to this scaling, whereas the uncertainty is propagated into the Hα luminosity. The Na I D EW, 3.7 ± 0.2 Å, gives a first-guess $T_{\rm eff} \approx 4850$ K from the Tripicchio et al. (1997) relation. Its intrinsic ∼ 300 K scatter and unmodelled gravity and metallicity effects make it consistent with 4551 ± 150 K.

Over 5000–9000 Å, the continuum slope formally favours $A_V \sim 0.6$, but the optical estimate is imperfect. Beyond 8000 Åthe calibration is affected by increased uncertainty in the red response correction. We therefore retained the SED value $A_V = 0.171 \pm 0.050$ mag (van Capelleveen et al. 2025).

Appendix D: Accretion-luminosity derivation

A Monte Carlo calculation ($N = 10^5$) samples the photospheric-EW systematic, observed EW, continuum flux, 5% absolute scaling, A_V, distance, and the 0.13 dex Alcalá et al. (2017) scatter. Negative excesses are retained as zero accretion luminosity. We obtain $F_{\rm H\alpha,exc} = (3.5 \pm 1.9) \times 10^{-14}$ erg s^{-1} cm^{-2}, $\log L_{\rm H\alpha}/L_\odot = -4.67^{+0.19}_{-0.31}$, and $\log L_{\rm acc}/L_\odot = -3.54^{+0.26}_{-0.37}$. This lies ≃ 1.1 dex below the Manara et al. (2013) chromospheric-noise level. Interpreting all filling as accretion would give $\dot{M}_{\rm acc} = 1.4^{+1.2}_{-0.8} \times 10^{-11}$ $M_\odot$ yr^{-1}; because the filling is marginal and chromospheric, we instead adopt the 95% upper limit stated in Sect. 3.4.

Appendix E: Lithium equivalent width and age comparison

The unresolved Li I 6708 Åblend was measured in the three Grism 8 exposures. Each spectrum was continuum-normalised over 6680–6698 and 6717–6740 Å, and fitted over 6703–6711.5 Åwith $1 - f_{\rm norm}(\lambda) = A \exp[-(\lambda - \lambda_0)^2/(2\sigma^2)]$, so EW $= A\sigma\sqrt{2\pi}$. The coarser Grism 7 exposure was excluded. The measurements are mutually consistent ($\chi^2 = 1.03$ for two degrees of freedom) and give EW(Li + Fe) = 0.344 ± 0.030 Å. Subtracting a 10 mÅFe I/CN correction yields EW(Li) = 0.334 ± 0.030 Å, an approximate upper limit at this resolution.

Table E.1. Li I 6708 Åequivalent width measurements.

Spectrum	$t_{\rm exp}$ (s)	EW(Li+Fe) (Å)	$\sigma_{\rm EW}$ (Å)
ajd14044	600	0.317	0.046
ajd14045	600	0.389	0.055
ajd14047	300	0.340	0.054
Weighted mean		0.344	0.030

The fitted FWHM (4.8–5.7 Å) confirms that the doublet and neighbouring blend are unresolved. At $T_{\rm eff} \simeq 4551$ K the measured EW lies near the upper Pleiades envelope, but blending and the intrinsic factor-of-two spread among K dwarfs prevent a precise age constraint (Martín 1997; Bouvier et al. 2018; Somers & Pinsonneault 2017). Lithium therefore supports youth, but does not independently establish the ∼ 5 Myr age, which rests on the SED–isochrone fit and Theia 53 membership (van Capelleveen et al. 2025).

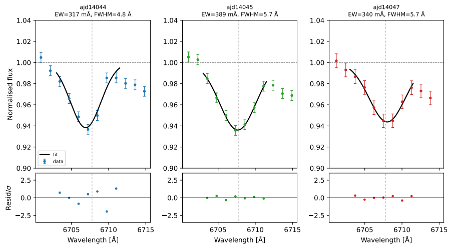

Fig. E.1. Gaussian fits to the Li I 6708 Åblend in the three Grism 8 exposures (top) and residuals normalised by the per-pixel noise (bottom). The dotted line marks 6707.78 Å.